

Disorder-induced half-integer quantized conductance plateau in quantum anomalous Hall insulator–superconductor structures

Yingyi Huang,^{1,2} F. Setiawan,¹ and Jay D. Sau¹

¹*Department of Physics, Condensed Matter Theory Center and Joint Quantum Institute, University of Maryland, College Park, Maryland 20742, USA*

²*State Key Laboratory of Optoelectronic Materials and Technologies, School of Physics, Sun Yat-sen University, Guangzhou 510275, China*

(Dated: June 21, 2022)

Weak superconducting proximity effect in the vicinity of the topological transition of a quantum anomalous Hall system has been proposed as a venue to realize a topological superconductor (TSC) with chiral Majorana edge modes. Recently, experimental evidence of such chiral Majorana modes has been observed in the form of a half-integer quantized plateau in the two-terminal transport measurement of a quantum anomalous Hall–superconductor junction. While we agree with previous theoretical work that the presence of superconducting proximity effect generically splits the quantum Hall transition into two phase transitions with a gapped $\mathcal{N} = 1$ TSC in between, in this work we propose that a nearly flat conductance plateau, similar to that expected from chiral Majorana modes, can also arise from the interplay of percolation of quantum Hall edges well before the onset of the TSC and also at temperatures much above the gap of the TSC. Our work, therefore, suggests that in order to confirm the TSC, it is necessary to either observe perfectly quantized conductance plateau at very low temperatures or supplement the conductance measurements with heat transport signatures that would ensure the presence of a spectral gap underneath the superconducting region.

Recent years have seen a burgeoning interest in realizing topological superconductors (TSCs) which host zero-energy Majorana modes. These Majorana zero modes are not only of fundamental interest but also hold potential applications for a fault-tolerant topological quantum computation [1] owing to their non-Abelian braiding statistics [2, 3]. The Majorana modes can be found in the vortex cores of a two-dimensional (2D) chiral TSCs with an odd integer Chern number. Recent theoretical studies [4–6] proposed to realize this chiral TSC using a quantum anomalous Hall insulator (QAHI) in proximity to an *s*-wave superconductor (SC).

The quantum anomalous Hall (QAH) state is a quantum Hall (QH) state without an external magnetic field which can be realized in a 2D thin film of magnetic topological insulator (TI) with ferromagnetic ordering [7–11]. For the regime where the ferromagnetic-induced exchange field strength $|\lambda|$ is greater than the hybridization gap $|m_0|$ induced by the coupling between the top and bottom surfaces, the system has a Chern number $\mathcal{C} = \lambda/|\lambda|$ and in the opposite limit where $|\lambda| < |m_0|$, $\mathcal{C} = 0$ [6, 12]. By changing the applied magnetic field over a relatively small range, a topological phase transition can be induced between the QAHI with $\mathcal{C} = 1$ and the trivial insulator state with $\mathcal{C} = 0$ [13]. When the QAH is proximitized by an *s*-wave SC, the $\mathcal{C} = 1$ and $\mathcal{C} = 0$ phases are driven into $\mathcal{N} = 2$ and $\mathcal{N} = 0$ TSC, respectively. At the transition between these two phases, there exists an $\mathcal{N} = 1$ TSC [4, 5]. This TSC has a full pairing bulk gap and $\mathcal{N} = 1$ gapless chiral Majorana edge mode (CMEM) at the edge. Since the CMEM carries one-half of the incoming charges, it manifests as a half-integer quantized plateau $e^2/2h$ in the conductance

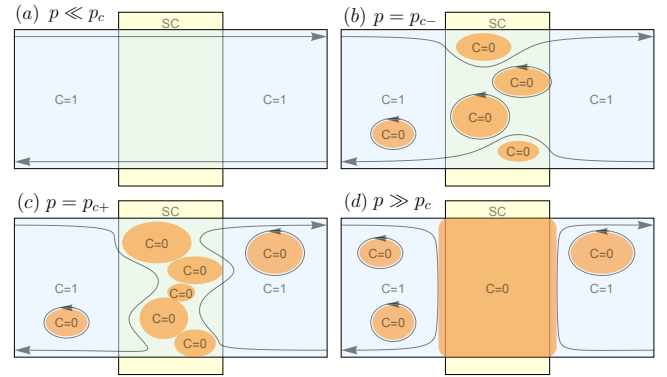


FIG. 1. (Color online) Schematics of the magnetic-field induced percolation in a disordered QAHI-SC-QAHI junction. The middle QAHI region is proximitized by an *s*-wave SC (yellow rectangle). Four different percolation stages of trivial insulator phases with $\mathcal{C} = 0$ (orange region) in the QAHI phase with $\mathcal{C} = 1$ (light-blue region). These four stages are characterized by different values of p , the proportion of $\mathcal{C} = 0$ phase, which changes with magnetic field. (a) In the strong magnetic field regime where p is far below the percolation threshold ($p \ll p_c$), the system is in the $\mathcal{C} = 1$ phase. The edge states (shown by arrowed lines) are perfectly transmitted across the junction. (b) During the magnetization reversal, the $\mathcal{C} = 0$ phase domains grow. The edge states wind around the domains in the superconducting region. (c) When p is slightly above the percolation threshold ($p = p_{c+}$), the domains are connected across the width of the junction and the edge states can no longer be transmitted across the junction. (d) When $p \gg p_c$, the edge states are normally reflected by the $\mathcal{C} = 0$ phase in the SC region.

measured between two normal leads and an integer quantized e^2/h peak in the conductance between a normal

lead and the SC during the magnetization reversal. Recent experiment [14] observed these two transport signatures in a doped magnetic QAHI thin film proximitized by an s -wave SC [5, 6]. While these transport signatures are consistent with the existence of an $\mathcal{N} = 1$ TSC with a single CMEM for a clean system, the experimental system, however, is disordered with a subgap density of states that may lower the gap of the $\mathcal{N} = 1$ TSC or shrink the phase space over which it is realized.

In this Letter, we show that these two transport signatures can generically occur in a disordered QAHI-SC-QAHI junction even in phases where the CMEM is absent such as in the $\mathcal{C} = 1$ phase. Here, the SC region is the QAHI placed in proximity to an s -wave SC. We consider the system to be inhomogeneous but with smoothly varying magnetization [15]. It was argued in Ref. [16] that these inhomogeneity-induced domain walls are required to understand the transport properties in the QAHI-SC-QAHI system such as the Hall conductance. Figure 1 shows the evolution of the phases in the QAHI state as the magnetic field is varied. In the limit of strong magnetic field, the system is in a single-domain $\mathcal{C} = 1$ phase [as shown in Fig. 1(a)] with large average magnetization. In this regime, the edge states are perfectly transmitted across the junction. During the magnetization reversal, the proportion p of the $\mathcal{C} = 0$ domain increases where the average magnetization in the $\mathcal{C} = 0$ domain is small. Since the chiral edge states lives in the boundary between the $\mathcal{C} = 0$ and $\mathcal{C} = 1$ domains, the edge state has to wind around the $\mathcal{C} = 0$ domain which increases and decreases its Andreev and normal scattering probabilities, respectively. As p approaches the percolation threshold p_c (where the $\mathcal{C} = 0$ domains become connected into a cluster spanning across the width of the junction), the electron trajectory $L \rightarrow \infty$. As a result, at $p = p_c$, the electron at zero energy undergoes equal amount of normal and Andreev scattering processes giving rise to an $e^2/2h$ two-terminal conductance plateau. As p increases above p_c , L becomes shorter which in turn increases and decreases the normal and Andreev scattering probabilities, respectively. For $p \gg p_c$, the system is in the $\mathcal{C} = 0$ phase and electrons undergo perfect normal reflections outside the superconducting region as shown in Fig. 1(d).

We describe the low-energy edge modes of the QAHI-SC structure by a one-dimensional Hamiltonian:

$$H(x) = \frac{1}{2} \int dx \mathcal{C}^\dagger(x) \mathcal{H}_{\text{BdG}}(x) \mathcal{C}(x), \quad (1)$$

where

$$\mathcal{H}_{\text{BdG}}(x) = -iv\tau_0\partial_x - \mu(x)\tau_z + \frac{1}{2} \{-i\partial_x, \Delta(x)\tau_x\} \quad (2)$$

is the Bogoliubov-de Gennes (BdG) Hamiltonian and $\mathcal{C}(x) = (c(x), c^\dagger(x))^T$ is the Nambu spinor with $c(x)$ and $c^\dagger(x)$ being the electron annihilation and creation operators, respectively. Here, v is the edge mode velocity, μ

is the chemical potential, Δ is the effective p -wave pairing potential of the proximity-induced superconductivity, $\tau_{x,y,z}$ are the Pauli matrices acting on the particle-hole space. For simplicity, we work in the units where the Planck constant \hbar , Boltzmann constant k_B and edge velocity v are set to 1. We note that the term ∂_x in the Hamiltonian comes with the anticommutation relation $\{\cdot, \cdot\}$ to ensure the Hermiticity of the Hamiltonian. The p -wave pairing amplitude $\Delta(x)$ is induced from the proximity effect of an s -wave SC with amplitude $\Delta_0(x)$. This cannot occur in a strictly spin-polarized edge state. However, since the QAHI system arises from a TI, which is a strongly spin-orbit-coupled system, we expect the spin-polarization of the chiral edge state to vary with momentum (similar to the spin-texture in a TI [17] on a scale of the spin-orbit length k_{so}^{-1} where k_{so} is related to the exchange field λ by $k_{\text{so}} \sim \lambda/v$). Within this model we then have $\Delta(x) \sim v\Delta_0(x)/\lambda$ (see Supplemental Material [18] for the derivation).

We consider a QAHI-SC-QAHI junction (see Fig. 1) with spatially varying $\mu(x)$ and $\Delta(x)$ which naturally occurs in typical doped QAHI systems. For the QAHI region, we set $\mu = \Delta = 0$, while for the SC region, we set $\mu(x)$ and $\Delta(x)$ to be spatially varying along the electron trajectory length L (see Supplemental Material [19] for the spatial profile).

We can write down the scattering matrix at energy E which relates the incoming and outgoing modes at the QAHI-SC boundaries as

$$\mathcal{S}(E) = \begin{pmatrix} s_N(E) & s_A^*(-E) \\ s_A(E) & s_N^*(-E) \end{pmatrix}, \quad (3)$$

where

$$\mathcal{S} = \begin{cases} \mathcal{T}, & \text{for } p < p_c, \\ \mathcal{R}, & \text{for } p > p_c, \end{cases} \quad (4)$$

with \mathcal{T} and \mathcal{R} denoting the coherence transmission and reflection, respectively. Note that the reflection and transmission matrices can be written separately as the edge states do not couple to each other. As a result, they can either be transmitted (i.e., $\mathcal{T} = \mathcal{S}$ and $\mathcal{R} = 0$) for $p < p_c$ or reflected (i.e., $\mathcal{R} = \mathcal{S}$ and $\mathcal{T} = 0$) for $p > p_c$. The scattering matrix elements can be calculated by matching the incoming and outgoing modes in the SC region (see Supplemental Material [19] for the derivation), which yields

$$\mathcal{S}(E) = \prod_j e^{i\tilde{v}_j^{-1/2}(\mu_j\tau_z + E\tau_0)\tilde{v}_j^{-1/2}\ell}, \quad (5)$$

where $\tilde{v}_j = v\tau_0 + \Delta_j\tau_x$ is the effective edge mode velocity along region j with chemical potential μ_j and pairing potential Δ_j and ℓ is the lattice cutoff parameter. Since the scattering matrix in the QAHI region gives just a

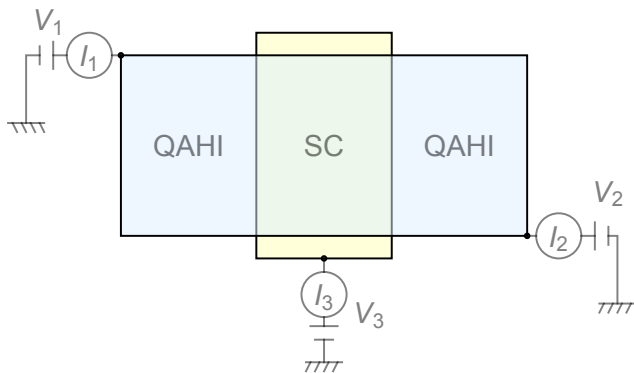


FIG. 2. (Color online) Schematic diagram of the setup used to measure the conductance in a QAHI-SC-QAHI junction. For the case where G_{12} is measured, we consider the SC to be floating (i.e., the current $I_3 = 0$) and the voltages V_1 and V_2 to be applied to leads 1 and 2, respectively. For the case where G_{13} is measured, the SC is grounded (i.e., $I_3 \neq 0$), lead 2 is removed, the voltages V_1 and V_3 are applied to leads 1 and SC, respectively.

trivial phase factor in the current amplitude, the length of QAHI region does not change the conductance and hence can be ignored in the calculation.

We study the conductance within the linear response where the voltage is near zero energy. The conductance of the junction is related to the difference between the zero-temperature normal and Andreev scattering probabilities $\delta S_0(E) = |s_N(E)|^2 - |s_A(E)|^2$. At finite temperature T , δS at zero energy can be computed from the zero-temperature $\delta S_0(E)$ by a convolution with the derivative of Fermi distribution, i.e.,

$$\delta S = \int dE \left(-\frac{\partial f_T(E)}{\partial E} \right) (|s_N(E)|^2 - |s_A(E)|^2), \quad (6)$$

where $f_T(E) = 1/(e^{(E-\mu_{\text{QAHI}})/T} + 1)$ is the Fermi distribution with $\mu_{\text{QAHI}} = 0$ being the chemical potential of the QAHI.

The conductance is measured using the setup shown in Fig. 2. Within the generalized Landauer-Büttiker transport formalism for a normal-superconductor interface [20, 21], the current flowing in leads 1 and 2 are given by

$$I_1 = \frac{e^2}{h} [(1 - \delta\mathcal{R})(V_1 - V_3) - \delta\mathcal{T}(V_2 - V_3)], \quad (7a)$$

$$I_2 = \frac{e^2}{h} [-\delta\mathcal{T}'(V_1 - V_3) + (1 - \delta\mathcal{R}')(V_2 - V_3)], \quad (7b)$$

where V_1 and V_2 are the voltages applied to leads 1 and 2, respectively, and V_3 is the voltage of the SC which is set to 0. Here, $\delta\mathcal{R}$ and $\delta\mathcal{T}$ are the net reflection and transmission probabilities for the left-incoming electron, respectively while $\delta\mathcal{R}'$ and $\delta\mathcal{T}'$ are the net reflection and transmission probabilities for the right-incoming electron, respectively.

We consider two kinds of measurement setups: floating and grounding SC. For the case of floating SC, there is no current flowing from the SC to the ground ($I_3 = 0$). Using Eq. (7) and the current conservation equation ($I_1 + I_2 = 0$), we obtain the conductance between leads 1 and 2 as

$$G_{12} \equiv \frac{I_1}{V_1 - V_2} = \frac{e^2}{h} \left[\frac{\delta\mathcal{T}\delta\mathcal{T}' - (1 - \delta\mathcal{R})(1 - \delta\mathcal{R}')}{\delta\mathcal{T} + \delta\mathcal{T}' + \delta\mathcal{R} + \delta\mathcal{R}' - 2} \right]. \quad (8)$$

For the second case where the SC is grounded, there is a current flowing from the SC to the ground ($I_3 \neq 0$). For this scheme, we consider removing lead 2 ($I_2 = 0$). Applying Eq. (7) for this case, we obtain the conductance between lead 1 and SC as

$$G_{13} \equiv \frac{I_1}{V_1 - V_3} = \frac{e^2}{h} \left[\frac{(1 - \delta\mathcal{R})(1 - \delta\mathcal{R}') - \delta\mathcal{T}\delta\mathcal{T}'}{1 - \delta\mathcal{R}'} \right]. \quad (9)$$

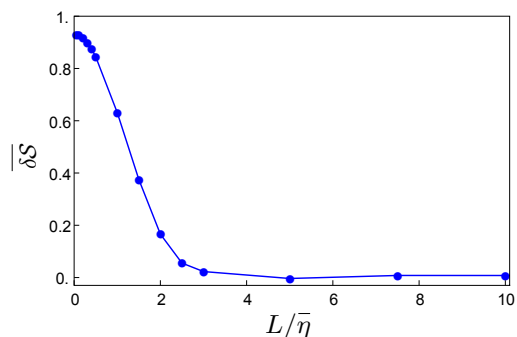


FIG. 3. (Color online) Disorder-averaged zero-energy net scattering probability ($\bar{\delta S} = \overline{|s_N|^2 - |s_A|^2}$), which is the difference between the normal and Andreev scattering probabilities, as a function of electron trajectory length $L/\bar{\eta}$ where $\bar{\eta} = v/\bar{\Delta}$ is a dimensionless disorder-averaged superconducting coherence length. Note that $\bar{\delta S}$ exponentially decays with L . For $p < p_c$, there is only coherence transmission process ($\delta S = \delta\mathcal{T}$ and $\delta\mathcal{R} = 0$), while for $p > p_c$, there is only coherence reflection process ($\delta S = \delta\mathcal{R}$ and $\delta\mathcal{T} = 0$). We consider the disorder in Δ and μ where the values of $\Delta \in [0, 0.1]$ and $\mu \in [-0.01, 0.01]$ are drawn from uniform distributions. Parameters used are edge mode velocity $v = 1$ and temperature $T = 0.3$.

To understand how the percolation picture shown in Fig. 1 gives rise to a half-integer quantized conductance plateau in G_{12} and an integer quantized conductance peak in G_{13} , let us first look at the difference between the disorder-averaged zero-energy normal and Andreev scattering probabilities $\bar{\delta S}$ (calculated using Eq. (10)) as a function of the electron trajectory length $L/\bar{\eta}$ as plotted in Fig. 3 where $\bar{\eta} = vk_{\text{so}}/\Delta_0(x)$ is the disorder-averaged dimensionless superconducting coherence length. Note that the superconducting coherence length is dimensionless because of the p -wave pairing, which makes it essential to introduce the scale $k_{\text{so}} \sim (50 \text{ nm})^{-1}$. From Fig. 3,

we can see that $\overline{\delta S}$ decays exponentially with L . This exponential decay can be understood by first rewriting the scattering matrix \mathcal{S} in the Majorana basis. In this basis, \mathcal{S} is the average of product of random SO(2) matrices which can be mapped into random walks on a circle. As a result, we have

$$\overline{\delta S} = \overline{|s_N|^2 - |s_A|^2} = \overline{\cos^2 \theta - \sin^2 \theta} \sim \exp(-2L\sigma^2/\ell) \quad (10)$$

where σ is the standard deviation of the angle θ that parametrizes the SO(2) matrix (see Supplementary material [22] for a proof).

The electron trajectory length L , which is the outer perimeter of a cluster comprising the connected $\mathcal{C} = 0$ domains, increases as the proportion $p \rightarrow p_c$ where the percolation threshold p_c corresponds to the magnetic field near the coercive field. Near p_c , L obeys the scaling relation [23]:

$$L = L_0 |p - p_c|^{-(1+\nu)d_f}. \quad (11)$$

Here, the correlation length exponent ν is $\frac{4}{3}$ [24], the fractal dimension of the cluster d_f is $\frac{91}{48}$ [25] for two dimensions.

From $\overline{\delta S}$ shown in Fig. 3, we calculated the disorder averaged conductances \overline{G}_{12} and \overline{G}_{23} using Eqs. (8) and (9), respectively. Figure 4 shows the numerically calculated \overline{G}_{12} and \overline{G}_{13} as a function of $p - p_c$ near the percolation threshold p_c . As seen from the plot, the conductance $\overline{G}_{12} \simeq e^2/h$ for $p < p_c$ and $\overline{G}_{12} \simeq 0$ for $p > p_c$ with a exponentially flat plateau at $e^2/2h$ near p_c while the conductance $\overline{G}_{13} \simeq 0$ for $p < p_c$ and $p > p_c$ with a peak at e^2/h near p_c . Near p_c , we can write \overline{G}_{12} and \overline{G}_{13} by using Eqs. (8)-(11) as

$$\overline{G}_{12} \approx \begin{cases} \frac{e^2}{2h} (1 + e^{-2\alpha|p-p_c|^{-(1+\nu)d_f}}), & \text{for } p = p_{c-}, \\ \frac{e^2}{2h} (1 - e^{-2\alpha|p-p_c|^{-(1+\nu)d_f}}), & \text{for } p = p_{c+}, \end{cases} \quad (12)$$

and

$$\overline{G}_{13} \approx \begin{cases} \frac{e^2}{h} (1 - e^{-4\alpha|p-p_c|^{-(1+\nu)d_f}}), & \text{for } p = p_{c-}, \\ \frac{e^2}{h} (1 - e^{-2\alpha|p-p_c|^{-(1+\nu)d_f}}), & \text{for } p = p_{c+}, \end{cases} \quad (13)$$

where $\alpha = L_0\sigma^2/\ell$. We note that even though \overline{G}_{12} and \overline{G}_{13} are perfectly quantized at $e^2/2h$ and e^2/h , respectively, only when $p = p_c$, there are exponentially flat plateaus at these quantized values. These two conductance plateaus, which originate from the disorder effect, resemble the experimental data [14] claimed to be the signatures of CMEMs.

Our results, based on a classical percolation model for the QH transition, are valid at high temperatures where the chiral edge becomes effectively long enough to produce the plateaus in Fig. 4. This classical percolation

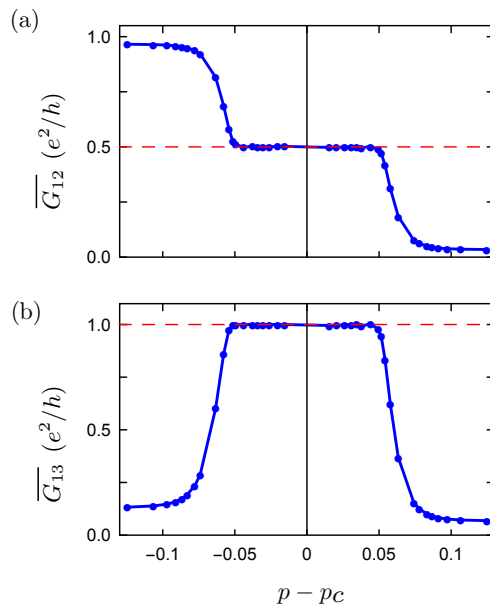


FIG. 4. (Color online) Disorder-averaged conductance (a) \overline{G}_{12} and (b) \overline{G}_{13} as a function of p near the percolation threshold p_c . The parameters used here are the same as those used in Fig. 3. \overline{G}_{12} exhibits a half-integer quantized plateau near p_c while \overline{G}_{13} shows an integer quantized peak near p_c . We set L_0 in Eq. (11) to be $500\overline{\eta}$ such that the conductance plateaus width is in a small region near p_c .

picture is a reasonable description of the QH transition away from the critical point or at a relatively high temperature [15] or in the presence of dissipation that can arise from interplay of interaction, disorder and temperature [26]. Finite temperature is also crucial for allowing us to consider a disorder averaging for the transmission probabilities. Technically, a single system with elastic impurity scatterings is a fixed disorder realization and would lead to strong mesoscopic fluctuations in the transmission probability. Thermal noise leads to time-dependent fluctuations of the disorder potential that are averaged over justifying the averaging.

Let us now discuss how our calculated conductance would vary with lowering temperature. Ideally, the presence of an SC splits the QH transition ($\mathcal{N} = 2$ to $\mathcal{N} = 0$) into two phase transitions with a gapped $\mathcal{N} = 1$ TSC in between. The near $e^2/2h$ plateau in Fig. 4 that we calculate at high temperatures would describe results not only outside the range of the $\mathcal{N} = 1$ phase as described but also in the $\mathcal{N} = 1$ phase for temperatures above the topological gap. At such high temperatures $\overline{\delta S}$ would vanish because the edge quasiparticles could escape into the bulk by thermal excitations. In principle, observing the stabilization of the plateau to a more perfectly quantized plateau as temperature is lowered would be a signature of an $\mathcal{N} = 1$ TSC. Furthermore, an observation of the superconducting gap is also necessary in order to

rule out the percolation mechanism of the edge states due to the formation of the metallic phases at the transition. Additionally, it has been proposed that in the limit of strong disorder the gapped $\mathcal{N} = 1$ TSC may be replaced by a gapless Majorana metal phase even at zero temperature [27]. Such a scenario similar to the dissipative metallic phase would allow the validation of the classical percolation results that led to Fig. 4 and have a similar $e^2/2h$ plateau.

Using the percolation picture, we have shown that a nearly half-integer quantized conductance plateau in \overline{G}_{12} and a nearly integer quantized conductance peak in \overline{G}_{13} can arise even in the conventional QAHI (i.e., $\mathcal{N} = 2$) phase in a disordered QAHI-SC-QAHI junction. A similar conductance plateau can also arise in the $\mathcal{N} = 1$ TSC phase at temperatures well above the TSC gap. While our results (Fig. 4) do not contradict the theoretical existence of the TSC phase (which is likely though not inevitable) in the vicinity of the QAH transition, the exponentially flat $e^2/2h$ conductance plateau makes it difficult to establish the experimental observation [14] as strong experimental evidence for the $\mathcal{N} = 1$ TSC. For example, the $\mathcal{N} = 1$ TSC at a temperature above the topological gap has no observable non-Abelian particles making it difficult to connect the conductance plateau to topological properties. A smoking-gun test for the $\mathcal{N} = 1$ TSC would be to measure the associated thermal Hall conductivity of the system. A measurement of the thermal conductance or heat capacity would reveal if the system underneath the SC is truly in a gapped phase in the putative topological region as opposed to the gapless phase considered in this manuscript. Both the classical percolation-based model as well as the Majorana metal phase would have large longitudinal thermal conductance and make the thermal Hall conductance non-universal.

We thank K. T. Law for valuable discussions that drew our attention to Ref. [14] which motivated this work. J.S. acknowledges stimulating discussion with S.-C. Zhang that motivated the discussion of the low-temperature limit. We also thank Yahya Alavirad, Ching-Kai Chiu and Qing Lin He for helpful discussions. This work is supported by JQI-NSF-PFC. Y.H. is grateful to China Scholarship Council for financial support. J.D.S. acknowledges the funding from Sloan Research Fellowship and NSF-DMR-1555135 (CAREER). We acknowledge the University of Maryland supercomputing resources (<http://www.it.umd.edu/hpcc>) made available in conducting the research reported in this paper.

Note added Upon completion of our draft, we became aware of a recent manuscript [28] related to our work.

-
- [1] C. Nayak, S. H. Simon, A. Stern, M. Freedman, and S. Das Sarma, *Rev. Mod. Phys.* **80**, 1083 (2008).
 - [2] N. Read and D. Green, *Phys. Rev. B* **61**, 10267 (2000).
 - [3] D. A. Ivanov, *Phys. Rev. Lett.* **86**, 268 (2001).
 - [4] X.-L. Qi, T. L. Hughes, and S.-C. Zhang, *Phys. Rev. B* **82**, 184516 (2010).
 - [5] S. B. Chung, X.-L. Qi, J. Maciejko, and S.-C. Zhang, *Phys. Rev. B* **83**, 100512 (2011).
 - [6] J. Wang, Q. Zhou, B. Lian, and S.-C. Zhang, *Phys. Rev. B* **92**, 064520 (2015).
 - [7] X.-L. Qi, Y.-S. Wu, and S.-C. Zhang, *Phys. Rev. B* **74**, 085308 (2006).
 - [8] C.-X. Liu, X.-L. Qi, X. Dai, Z. Fang, and S.-C. Zhang, *Phys. Rev. Lett.* **101**, 146802 (2008).
 - [9] C.-X. Liu, S.-C. Zhang, and X.-L. Qi, *Annu. Rev. Condens. Matter Phys.* **7**, 301 (2016).
 - [10] R. Yu, W. Zhang, H.-J. Zhang, S.-C. Zhang, X. Dai, and Z. Fang, *Science* **329**, 61 (2010).
 - [11] C.-Z. Chang, J. Zhang, X. Feng, J. Shen, Z. Zhang, M. Guo, K. Li, Y. Ou, P. Wei, L.-L. Wang, *et al.*, *Science* **340**, 167 (2013).
 - [12] J. Wang, B. Lian, and S.-C. Zhang, *Phys. Rev. B* **89**, 085106 (2014).
 - [13] C.-Z. Chang, W. Zhao, J. Li, J. K. Jain, C. Liu, J. S. Moodera, and M. H. W. Chan, *Phys. Rev. Lett.* **117**, 126802 (2016).
 - [14] Q. L. He, L. Pan, A. L. Stern, E. C. Burks, X. Che, G. Yin, J. Wang, B. Lian, Q. Zhou, E. S. Choi, K. Murata, X. Kou, Z. Chen, T. Nie, Q. Shao, Y. Fan, S.-C. Zhang, K. Liu, J. Xia, and K. L. Wang, *Science* **357**, 294 (2017).
 - [15] J. Chalker and P. Coddington, *Journal of Physics C: Solid State Physics* **21**, 2665 (1988).
 - [16] C.-Z. Chen, J. J. He, D.-H. Xu, and K. T. Law, *Phys. Rev. B* **96**, 041118 (2017).
 - [17] M. Z. Hasan and C. L. Kane, *Rev. Mod. Phys.* **82**, 3045 (2010).
 - [18] See Sec. I of the Supplemental Material for the derivation of the effective p -wave pairing potential Δ from the minimal QAH two-band model.
 - [19] See Sec. II of the Supplemental Material for detailed derivations of the scattering matrix.
 - [20] M. P. Anantram and S. Datta, *Phys. Rev. B* **53**, 16390 (1996).
 - [21] O. Entin-Wohlman, Y. Imry, and A. Aharony, *Phys. Rev. B* **78**, 224510 (2008).
 - [22] See Sec. III of the Supplemental Material for a proof of the exponential decay of $\delta\overline{S}$ with L .
 - [23] M. B. Isichenko, *Rev. Mod. Phys.* **64**, 961 (1992).
 - [24] B. Nienhuis, *Phys. Rev. Lett.* **49**, 1062 (1982).
 - [25] A. Kapitulnik, A. Aharony, G. Deutscher, and D. Stauffer, *Journal of Physics A: Mathematical and General* **16**, L269 (1983).
 - [26] A. Kapitulnik, N. Mason, S. A. Kivelson, and S. Chakravarty, *Phys. Rev. B* **63**, 125322 (2001).
 - [27] T. Senthil and M. P. A. Fisher, *Phys. Rev. B* **61**, 9690 (2000).
 - [28] W. Ji and X.-G. Wen, arXiv:1708.06214 (2017).
 - [29] R. Jackiw and C. Rebbi, *Phys. Rev. D* **13**, 3398 (1976).
 - [30] S.-Q. Shen, *Topological insulators: Dirac Equation in Condensed Matters* (Springer-Verlag, Berlin Heidelberg, 2012).

Supplemental Material

I. DERIVATION OF EFFECTIVE p -WAVE PAIRING POTENTIAL Δ FROM THE MINIMAL TWO-BAND MODEL

In this appendix, we derive the p -wave superconducting pairing potential Δ from the minimal two-band model where we consider the superconducting term as a perturbation term in the Hamiltonian. The two band-model for the QAH is given by [6]

$$\mathcal{H}(\mathbf{k}) = -vk_x\zeta_z\sigma_y + vk_y\zeta_z\sigma_x + m_0\zeta_x + \lambda\sigma_z, \quad (\text{S-1})$$

with $\zeta_{x,y,z}$ and $\sigma_{x,y,z}$ being the Pauli matrices for layer and spin, respectively. Here, λ is the exchange field and m_0 is the hybridization gap. For $|\lambda| > |m_0|$, the system has a Chern number $\mathcal{C} = \lambda/|\lambda|$ and for $|\lambda| < |m_0|$, $\mathcal{C} = 0$.

The low-energy wave function of the Hamiltonian at $k_{x,y} = 0$ is given by $\psi_1 = 1/\sqrt{2}(0, 0, 1, 1)^T$ and $\psi_2 = 1/\sqrt{2}(-1, 1, 0, 0)^T$ with energies $E_1 = m_0 - \lambda$ and $E_2 = -m_0 + \lambda$, respectively. Projecting the Hamiltonian (Eq. (S-1)) into this low-energy subspace ($\psi_{1,2}$), we have

$$H(x) = -\tilde{m}(y)\rho_z - vk_y\rho_x - vk_x\rho_y \quad (\text{S-2})$$

where ρ is the Pauli matrix acting in the $\psi_{1,2}$ subspace. Since our aim is to derive the effective p -wave pairing potential for the edge state which lives at the boundary between the $\mathcal{C} = 0$ and $\mathcal{C} = 1$ domain, we consider the quantity $\tilde{m}(y) = \lambda - m_0(y)$ to change sign at $y = 0$ where

$$\tilde{m}(y) = \begin{cases} -\tilde{m}_1 & \text{for } y < 0 \\ \tilde{m}_2 & \text{for } y > 0 \end{cases} \quad (\text{S-3})$$

with $\tilde{m}_1, \tilde{m}_2 > 0$. Since the Hamiltonian is translationally invariant along x , the momentum k_x is a good quantum number. In the following, we focus on $k_x \approx 0$ where the Hamiltonian at $k_x = 0$ can be written as

$$H_0(y) = -\tilde{m}(y)\rho_z + iv\partial_y\rho_x. \quad (\text{S-4})$$

The above Hamiltonian admits a zero-energy Majorana mode at the boundary due to the fact that \tilde{m} changes sign at the boundary. The Schrödinger equation $H_0\phi = 0$ for the Majorana mode can be written as

$$\partial_y\phi(y) = -\frac{\tilde{m}(y)}{v}\rho_x\phi(y). \quad (\text{S-5})$$

Solving the above equation, we obtain [29, 30]

$$\phi_{\pm}(y) = \sqrt{\frac{\tilde{m}_1\tilde{m}_2}{v(\tilde{m}_1 + \tilde{m}_2)}} \begin{pmatrix} 1 \\ \pm i \end{pmatrix} \exp\left(\mp \int_0^y \frac{\tilde{m}(y')}{v} dy'\right), \quad (\text{S-6})$$

where ϕ_+ (ϕ_-) is the solution for $y > 0$ ($y < 0$). The wave function near $k_x = 0$ can be obtained from the first-order perturbation theory by treating the term $-vk_x\rho_y$ in Eq. (S-2) as the perturbation term. We note that the BdG wave function is given by $\Psi_{k_y}(x) = \begin{pmatrix} \psi_{k_y}(x) \\ \bar{\psi}_{k_y}(x) \end{pmatrix}$ where the particle- and hole-component of the wave function are related by $\bar{\psi}_{k_y}(x) = i\sigma_y\psi_{k_y}^*(x)$. The superconducting term is given by

$$\begin{aligned} \tilde{\Delta} &= \Delta_0 \int_{-\infty}^{\infty} dy \Psi_{-k_x}^\dagger(y) \tau_x \Psi_{k_x}(y), \\ &= \Delta_0 \int_{-\infty}^{\infty} dy \left[\psi_{-k_x}^\dagger(y) \bar{\psi}_{k_x}(y) + \bar{\psi}_{-k_x}^\dagger(y) \psi_{k_x}(y) \right], \\ &= \Delta_0 \int_{-\infty}^{\infty} dy \left[\psi_{-k_x}^\dagger(y) (i\sigma_y) \psi_{k_x}^*(y) + \psi_{-k_x}^T(y) (-i\sigma_y) \psi_{k_x}(y) \right], \\ &= \Delta_0 \int_{-\infty}^{\infty} dy \left([\psi_{-k_x}^T(y) (i\sigma_y) \psi_{k_x}(y)]^* - [\psi_{-k_x}^T(y) (i\sigma_y) \psi_{k_x}(y)] \right), \\ &= -2\Delta_0 \text{Im} \left[\int_{-\infty}^{\infty} dy \psi_{-k_x}^T(y) (i\sigma_y) \psi_{k_x}(y) \right], \end{aligned} \quad (\text{S-7})$$

where Δ_0 is the proximity-induced s -wave pairing potential. To solve Eq. (S-7), we first expand the wave function near $k_x = 0$ using the first-order perturbation theory with $-vk_x\rho_y$ being the perturbation term. The wave function is given by

$$\psi_{k_x}(y) = \phi(y) + vk_x\phi'(y). \quad (\text{S-8})$$

where $\phi' = \frac{1}{v} \frac{d\psi}{dk_x} \Big|_{k_x=0}$. Plugging this into Eq. (S-7), we have

$$\tilde{\Delta} = -2\Delta_0 \text{Im} \left(\int_{-\infty}^{\infty} dy \left[\phi^T(y) - vk_x\phi'^T(y) \right] (i\sigma_y) \left[\phi(y) + vk_x\phi'(y) \right] \right). \quad (\text{S-9})$$

Since $[\phi'^T(x)\sigma_y\phi(x)]^T = -\phi^T(y)\sigma_y\phi'(y)$ and $u^T\sigma_y u = 0$ due to the fact that σ_y is antisymmetric, we have

$$\Delta = -4v\Delta_0 \text{Im} \left(\int_{-\infty}^{\infty} dy \phi^T(y) (i\sigma_y) \phi'(y) \right), \quad (\text{S-10})$$

where $\Delta = \tilde{\Delta}/k_x$ is the effective p -wave pairing potential. To evaluate the integral in Eq. (S-10), we first calculate the first-order perturbed wave function $\phi'(y)$ which is given by

$$\phi'(y) = - \int_{-\infty}^{\infty} G(y, y') \rho_y \phi(y') dy', \quad (\text{S-11})$$

where the Green's function satisfy

$$(\tilde{m}(y)\rho_y + v\partial_y) G(y, y') = i\rho_x \delta(y - y'). \quad (\text{S-12})$$

We solve Eq. (S-12) by first considering $y' < 0$, where we obtain

$$G(y, y') = \exp \left(\int_{y'-\epsilon}^y -\frac{\tilde{m}(y'')}{v} \rho_y dy'' \right) G(y' - \epsilon, y'), \quad \text{for } y < y' < 0, \quad (\text{S-13a})$$

$$vG(y' + \epsilon, y') = vG(y' - \epsilon, y') + i\rho_x, \quad \text{for } y = y' < 0, \quad (\text{S-13b})$$

$$G(y, y') = \exp \left(\int_{y'+\epsilon}^y -\frac{\tilde{m}(y'')}{v} \rho_y dy'' \right) G(y' + \epsilon, y'), \quad \text{for } y' < y < 0, \quad (\text{S-13c})$$

$$G(y, y') = \exp \left(\int_0^y -\frac{\tilde{m}(y'')}{v} \rho_y dy'' \right) G(0, y'), \quad \text{for } y' < 0 < y \quad (\text{S-13d})$$

Since the Green's function vanishes for $y \rightarrow \pm\infty$, Eqs. (S-13a) and Eqs. (S-13d) imply that $G(y' - \epsilon, y')$ and $G(0, y')$ must be the left eigenmatrix of ρ_y with eigenvalue -1 and 1, respectively, i.e., $G(y' - \epsilon, y') = \begin{pmatrix} 1 & \\ & -i \end{pmatrix} \begin{pmatrix} a & b \\ c & d \end{pmatrix}$ and $G(0, y') = \begin{pmatrix} 1 & \\ & i \end{pmatrix} \begin{pmatrix} a & b \\ c & d \end{pmatrix}$. Solving Eq. (S-12) for $y' < 0$, we have

$$G(y, y') = \begin{cases} G_{-,1}(y, y') = \frac{1}{2v} \exp \left(\int_{y'-\epsilon}^y -\frac{\tilde{m}_1}{v} dy'' \right) \begin{pmatrix} 1 & -i \\ -i & -1 \end{pmatrix}, & \text{for } y < y' < 0, \\ G_{-,2}(y, y') = \frac{1}{2v} \exp \left(\int_{y'+\epsilon}^y -\frac{\tilde{m}_1}{v} dy'' \right) \begin{pmatrix} 1 & i \\ i & -1 \end{pmatrix}, & \text{for } y' < y < 0, \\ G_{-,3}(y, y') = \frac{1}{2v} \exp \left(\int_0^y -\frac{\tilde{m}_2}{v} dy'' \right) \exp \left(\frac{\tilde{m}_1}{v} y' \right) \begin{pmatrix} 1 & i \\ i & -1 \end{pmatrix}, & \text{for } y' < 0 < y. \end{cases} \quad (\text{S-14})$$

Solving Eq. (S-12) for $y' > 0$ yields

$$G(y, y') = \exp \left(\int_0^y -\frac{\tilde{m}(y'')}{v} \rho_y dy'' \right) G(0, y'), \quad \text{for } y \leq 0 < y', \quad (\text{S-15a})$$

$$G(y, y') = \exp \left(\int_{y'-\epsilon}^y -\frac{\tilde{m}(y'')}{v} \rho_y dy'' \right) G(y' - \epsilon, y'), \quad \text{for } 0 < y < y', \quad (\text{S-15b})$$

$$vG(y' + \epsilon, y') = vG(y' - \epsilon, y') + i\rho_x, \quad \text{for } y = y' > 0, \quad (\text{S-15c})$$

$$G(y, y') = \exp \left(\int_{y'+\epsilon}^y -\frac{\tilde{m}(y'')}{v} \rho_y dy'' \right) G(y' + \epsilon, y'), \quad \text{for } 0 < y' < y. \quad (\text{S-15d})$$

By matching the boundary condition for the Green's function (S-15), we then have

$$G(y, y') = \begin{cases} G_{+,1}(y, y') = \frac{1}{2v} \exp\left(\int_0^y -\frac{\tilde{m}_1}{v} dy''\right) \exp\left(-\frac{\tilde{m}_2}{v} y'\right) \begin{pmatrix} 1 & -i \\ -i & -1 \end{pmatrix}, & \text{for } y < 0 < y', \\ G_{+,2}(y, y') = \frac{1}{2v} \exp\left(\int_{y'-\epsilon}^y -\frac{\tilde{m}_2}{v} dy''\right) \begin{pmatrix} 1 & -i \\ -i & -1 \end{pmatrix}, & \text{for } 0 < y < y', \\ G_{+,3}(y, y') = \frac{1}{2v} \exp\left(\int_{y'+\epsilon}^y -\frac{\tilde{m}_2}{v} dy''\right) \begin{pmatrix} 1 & i \\ i & -1 \end{pmatrix}, & \text{for } 0 < y' < y. \end{cases} \quad (\text{S-16})$$

Using Eqs. (S-14) and (S-16) in Eq. (S-12), we can solve for $\phi'(y)$. For $y < 0$, we have

$$\begin{aligned} \phi'_-(y) &= \int_{-\infty}^{y-\epsilon} G_{-,2}(y, y') \rho_y \phi_-(y') dy' + \int_{y+\epsilon}^0 G_{-,1}(y, y') \rho_y \phi_-(y') dy' + \int_0^\infty G_{+,1}(y, y') \rho_y \phi_+(y') dy', \\ &= \frac{1}{2} \sqrt{\frac{\tilde{m}_1 \tilde{m}_2}{v(\tilde{m}_1 + \tilde{m}_2)}} \exp\left(\frac{\tilde{m}_1}{v} y\right) \left[\frac{1}{\tilde{m}_1} \begin{pmatrix} 1 \\ i \end{pmatrix} - \frac{1}{\tilde{m}_2} \begin{pmatrix} 1 \\ -i \end{pmatrix} \right], \end{aligned} \quad (\text{S-17})$$

and for $y > 0$, we obtain

$$\begin{aligned} \phi'_+(y) &= \int_{-\infty}^0 G_{-,3}(y, y') \rho_y \phi_-(y') dy' + \int_0^{y-\epsilon} G_{+,3}(y, y') \rho_y \phi_+(y') dy' + \int_{y+\epsilon}^\infty G_{+,2}(y, y') \rho_y \phi_+(y') dy', \\ &= \frac{1}{2} \sqrt{\frac{\tilde{m}_1 \tilde{m}_2}{v(\tilde{m}_1 + \tilde{m}_2)}} \exp\left(-\frac{\tilde{m}_2}{v} y\right) \left[\frac{1}{\tilde{m}_1} \begin{pmatrix} 1 \\ i \end{pmatrix} - \frac{1}{\tilde{m}_2} \begin{pmatrix} 1 \\ -i \end{pmatrix} \right]. \end{aligned} \quad (\text{S-18})$$

Finally, using Eqs. S-6, (S-17), and (S-18) in Eq. (S-10), we can write

$$\begin{aligned} \Delta &= -4v\Delta_0 \text{Im} \left[\int_{-\infty}^0 \phi_-(y)^T (i\sigma_y) \phi'_-(y) dy + \int_0^\infty \phi_+(y)^T (i\sigma_y) \phi'_+(y) dy \right], \\ &= -4\Delta_0 \frac{1}{(\tilde{m}_1 + \tilde{m}_2)} \left[\int_{-\infty}^0 \tilde{m}_2 \exp\left(2\frac{\tilde{m}_1}{v} y\right) dy + \int_0^\infty \tilde{m}_1 \exp\left(-2\frac{\tilde{m}_2}{v} y\right) dy \right], \\ &= -\frac{2v\Delta_0}{(\tilde{m}_1 + \tilde{m}_2)} \left(\frac{\tilde{m}_2}{\tilde{m}_1} + \frac{\tilde{m}_1}{\tilde{m}_2} \right). \end{aligned} \quad (\text{S-19})$$

Since $\tilde{m}_{1,2} \sim \lambda$, we have

$$\Delta \sim v\Delta_0/\lambda. \quad (\text{S-20})$$

II. SCATTERING MATRIX

Using the BdG Hamiltonian in Eq. (2), we can write the Schrödinger equation $\mathcal{H}_{\text{BdG}}\psi = E\psi$ for the edge state as

$$-i\tilde{v}(x)\partial_x\psi_E(x) = \left(E\tau_0 + \mu(x)\tau_z + \frac{1}{2}i\partial_x\tilde{v}(x) \right) \psi_E(x), \quad (\text{S-21})$$

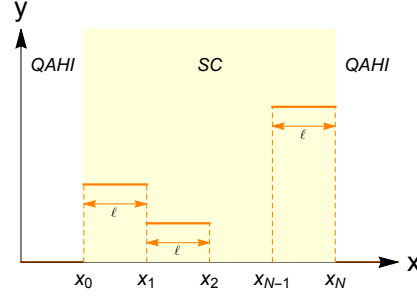
where $\tilde{v}(x) = v\tau_0 + \Delta(x)\tau_x$ is the effective edge mode velocity.

As shown in Fig. S1, we assume $\tilde{v}(x)$ to be spatially varying along the electron trajectory L in the SC region where $\tilde{v}(x)$ jumps at the boundaries (at $x = x_0, \dots, x_N$). Since $\partial_x\tilde{v}(x) \gg E, \mu$ at the boundaries, integrating Eq. (S-21) at the boundaries yields

$$\psi_E(x_{j+}) = \frac{\tilde{v}_j^{-1/2}}{\tilde{v}_{j+1}^{-1/2}} \psi_E(x_{j-}). \quad (\text{S-22})$$

Here, $x_{j\pm}$ is the position just to the right/left of the boundary j . In the region between x_{j-1} and x_j , $\tilde{v}(x) = \text{const}$, so we have

$$\psi_E(x_{j-}) = e^{i\tilde{v}_j^{-1}(\mu_j\tau_z + E\tau_0)\ell} \psi_E(x_{(j-1)+}). \quad (\text{S-23})$$



Supplementary Figure S1. (Color online) Spatial variation of μ, Δ along the electron trajectory L . The length over which Δ and μ remains constant is ℓ . For the numerical simulation done in this paper, we set $\ell = 0.05\bar{\eta}$.

Using the Baker-Campbell-Hausdorff formula $e^{iA^{-1}B} = A^{-1/2}e^{iA^{-1/2}BA^{-1/2}}A^{1/2}$, we can write down Eq. (S-23) as

$$\psi_E(x_{j-}) = \tilde{v}_j^{-1/2} e^{i\tilde{v}_j^{-1/2}(\mu_j\tau_z + E\tau_0)\tilde{v}_j^{-1/2}\ell} \tilde{v}_j^{1/2} \psi_E(x_{(j-1)+}). \quad (\text{S-24})$$

The outgoing current amplitude at $x_N = L$ is then given by

$$\mathcal{J}_{\text{out}}(E) = \prod_j^N e^{i\tilde{v}_j^{-1/2}(\mu_j\tau_z + E\tau_0)\tilde{v}_j^{-1/2}\ell} \mathcal{J}_{\text{in}}(E), \quad (\text{S-25})$$

where $\mathcal{J}_{\text{out}}(E) = \sqrt{v}\psi_E(x_N)$ and $\mathcal{J}_{\text{in}}(E) = \sqrt{v}\psi_E(x_0)$ are the outgoing and incoming current amplitudes in the SC region. The scattering matrix is given by

$$\mathcal{S}(E) = \prod_j^N e^{i\tilde{v}_j^{-1/2}(\mu_j\tau_z + E\tau_0)\tilde{v}_j^{-1/2}\ell}. \quad (\text{S-26})$$

III. PROOF FOR EXPONENTIAL DECAY OF $\overline{\delta S}$ WITH L

In the Majorana basis $\tilde{\mathcal{C}}_j \equiv \Lambda \mathcal{C}_j = \frac{1}{\sqrt{2}}(c_j + c_j^\dagger, ic_j - ic_j^\dagger)^T$ where $\Lambda = \frac{1}{\sqrt{2}} \begin{pmatrix} 1 & 1 \\ i & -i \end{pmatrix}$, the scattering matrix is given by $\tilde{\mathcal{S}} \equiv \Lambda \mathcal{S} \Lambda^\dagger$. Using the Baker-Campbell-Hausdorff formula $\Lambda e^A \Lambda^\dagger = e^{\Lambda A \Lambda^\dagger}$ and $\Lambda(\prod_j \mathcal{S}_j) \Lambda^\dagger = \prod_j (\Lambda \mathcal{S}_j \Lambda^\dagger)$ for unitary matrix Λ , we can write the scattering matrix as $\tilde{\mathcal{S}} \equiv \prod_j \tilde{\mathcal{S}}_j$. The zero-energy scattering matrix is then given by

$$\tilde{\mathcal{S}} = \prod_j^N \begin{pmatrix} \cos \theta_j & \sin \theta_j \\ -\sin \theta_j & \cos \theta_j \end{pmatrix} \quad (\text{S-27})$$

where $\theta_j = \frac{\mu\ell}{v\sqrt{1-\Delta_j^2}}$ and $N = L/\ell$.

Since $\tilde{\mathcal{S}}_j$ is real and unitary, it is in the $\text{SO}(2)$ group. The $\text{SO}(2)$ group has the following relation

$$\prod_j \tilde{\mathcal{S}}_j(\theta_j) = \tilde{\mathcal{S}}(\sum_j \theta_j), \quad (\text{S-28})$$

where $\theta_j \in [-\pi, \pi]$. If $\theta_1, \theta_2, \theta_3, \dots, \theta_N$ are independent and identically distributed random variables, each with mean $\bar{\theta}$ and variance σ^2 , for sufficiently large N the sum of the angle $\Theta = \sum_j \theta_j$, according to the central limit theorem, has a normal distribution $f(\Theta) = \frac{1}{\sqrt{2\pi N\sigma^2}} e^{-\frac{(\Theta - N\bar{\theta})^2}{2N\sigma^2}}$ with mean $\bar{\Theta} = N\bar{\theta}$ and variance $N\sigma^2$.

The net scattering probabilities is $\delta\tilde{\mathcal{S}} = |s_N|^2 - |s_A|^2 = \cos 2\Theta$ with its expectation value given by

$$\begin{aligned}
\overline{\delta\tilde{\mathcal{S}}} &= \int_{-N\pi}^{N\pi} f(\Theta) \cos(2\Theta) \\
&\approx -\frac{1}{4}e^{-2N\sigma^2} \cos(2N\bar{\theta}) \left(\operatorname{erf}\left(\frac{\sqrt{N}(\bar{\theta} - \pi)}{\sqrt{2}\sigma}\right) - \operatorname{erf}\left(\frac{\sqrt{N}(\bar{\theta} + \pi)}{\sqrt{2}\sigma}\right) \right) \\
&\approx \frac{1}{2}e^{-2N\sigma^2} \cos(2N\bar{\theta}) - \frac{\sigma \cos(2N\bar{\theta})}{2\sqrt{2N}\pi(\bar{\theta} + \pi)} e^{-\frac{N((\bar{\theta} + \pi)^2 + 4\sigma^4)}{2\sigma^2}} - \frac{\sigma \cos(2N\bar{\theta})}{2\sqrt{2N}\pi(\pi - \bar{\theta})} e^{-\frac{N((\bar{\theta} - \pi)^2 + 4\sigma^4)}{2\sigma^2}} + \mathcal{O}(N^{-3/2}e^{-N/2\sigma^2}).
\end{aligned} \tag{S-29}$$

Note that in the second line of Eq. (S-29) we have used $\sigma^2 \ll \pi$ and in the third line we only keep terms up to $\mathcal{O}(N^{-1/2}e^{-N/2\sigma^2})$. Since $e^{-2N\sigma^2}$ decays slower than $e^{-\frac{N((\bar{\theta} + \pi)^2 + 4\sigma^4)}{2\sigma^2}}$ and $e^{-\frac{N((\bar{\theta} - \pi)^2 + 4\sigma^4)}{2\sigma^2}}$ as $N \rightarrow \infty$, $\overline{\delta\tilde{\mathcal{S}}}$ is then given by

$$\overline{\delta\tilde{\mathcal{S}}} \propto e^{-2L\sigma^2/\ell}. \tag{S-30}$$

So $\overline{\delta\tilde{\mathcal{S}}}$ decays exponentially with the electron trajectory length L .